REPORT DOCUMENTATION PAGE

Form Approved OMB NO. 0704-0188

1. REPORT DATE (DD-MM-YYYY)	2. REPORT TYPE	3. DATES COVERED (From - To)
	New Reprint	-

4. TITLE AND SUBTITLE
Sharp Interface Algorithm for Large Density Ratio Incompressible Multiphase Magnetohydrodynamic Flows

5a. CONTRACT NUMBER
W911NF-13-1-0249

5b. GRANT NUMBER

5c. PROGRAM ELEMENT NUMBER
611102

6. AUTHORS
Tongfei Guo, Shuqiang Wang, Roman Samulyak

5d. PROJECT NUMBER

5e. TASK NUMBER

5f. WORK UNIT NUMBER

7. PERFORMING ORGANIZATION NAMES AND ADDRESSES
Research Foundation of SUNY at Stony Brc
Office of Sponsored Programs

West Sayville, NY 11796 -3362

8. PERFORMING ORGANIZATION REPORT NUMBER

9. SPONSORING/MONITORING AGENCY NAME(S) AND ADDRESS (ES)
U.S. Army Research Office
P.O. Box 12211
Research Triangle Park, NC 27709-2211

10. SPONSOR/MONITOR'S ACRONYM(S)
ARO

11. SPONSOR/MONITOR'S REPORT NUMBER(S)
63848-MA.2

12. DISTRIBUTION AVAILIBILITY STATEMENT
Approved for public release; distribution is unlimited.

13. SUPPLEMENTARY NOTES
The views, opinions and/or findings contained in this report are those of the author(s) and should not contrued as an official Department of the Army position, policy or decision, unless so designated by other documentation.

14. ABSTRACT
A numerical algorithm and the corresponding paralleled implementation for the study of magnetohydrodynamics (MHD) of large density ratio, three-dimensional multiphase flows at low magnetic Reynolds numbers have been developed. The algorithm employs the method of front tracking for the propagation of material interfaces and the embedded interface method for solving elliptic-parabolic problems associated with approximations of incompressible fluids and low magnetic Reynolds numbers. The use of embedded interface method supports arbitrary discontinuities of density and other physics properties across interfaces and significantly improves

15. SUBJECT TERMS
Front tracking; Multiphase MHD; Liquid metal MHD

16. SECURITY CLASSIFICATION OF:			17. LIMITATION OF ABSTRACT	15. NUMBER OF PAGES	19a. NAME OF RESPONSIBLE PERSON
a. REPORT	b. ABSTRACT	c. THIS PAGE			James Glimm
UU	UU	UU	UU		19b. TELEPHONE NUMBER 631-632-8370

Report Title

Sharp Interface Algorithm for Large Density Ratio Incompressible Multiphase Magnetohydrodynamic Flows

ABSTRACT

A numerical algorithm and the corresponding paralleled implementation for the study of magnetohydrodynamics (MHD) of large density ratio, three-dimensional multiphase flows at low magnetic Reynolds numbers have been developed. The algorithm employs the method of front tracking for the propagation of material interfaces and the embedded interface method for solving elliptic-parabolic problems associated with approximations of incompressible fluids and low magnetic Reynolds numbers. The use of embedded interface method supports arbitrary discontinuities of density and other physics properties across interfaces and significantly improves methods that smear interface discontinuities across several grid cells. The numerical algorithm has been implemented as an MHD extension of FronTier, a parallel front tracking hydrodynamic code, verified using asymptotic solutions and validated through the comparison with experiments on liquid metal jets. The FronTier-MHD code has been used for simulations of liquid mercury targets for the proposed muon collider / neutrino factory, ablation of pellets in tokamaks, and processes in hybrid magnetoinertial fusion.

REPORT DOCUMENTATION PAGE (SF298)
(Continuation Sheet)

Continuation for Block 13

ARO Report Number 63848.2-MA
Sharp Interface Algorithm for Large Density Rat...

Block 13: Supplementary Note

Approved for public release; distribution is unlimited.

Available online at www.sciencedirect.com

SciVerse ScienceDirect

Procedia Computer Science 18 (2013) 511 – 520

Procedia Computer Science

International Conference on Computational Science, ICCS 2013

Sharp Interface Algorithm for Large Density Ratio Incompressible Multiphase Magnetohydrodynamic Flows

Tongfei Guo[a], Shuqiang Wang[b], Roman Samulyak[a,b,*]

[a]*Department of Applied Mathematics and Statistics, Stony Brook University, Stony Brook, NY 11794, USA*
[b]*Computational Science Center, Brookhaven National Laboratory, Upton, NY 11973*

Abstract

A numerical algorithm and the corresponding paralleled implementation for the study of magnetohydrodynamics (MHD) of large density ratio, three-dimensional multiphase flows at low magnetic Reynolds numbers have been developed. The algorithm employs the method of front tracking for the propagation of material interfaces and the embedded interface method for solving elliptic-parabolic problems associated with approximations of incompressible fluids and low magnetic Reynolds numbers. The use of embedded interface method supports arbitrary discontinuities of density and other physics properties across interfaces and significantly improves methods that smear interface discontinuities across several grid cells. The numerical algorithm has been implemented as an MHD extension of FronTier, a parallel front tracking hydrodynamic code, verified using asymptotic solutions and validated through the comparison with experiments on liquid metal jets. The FronTier-MHD code has been used for simulations of liquid mercury targets for the proposed muon collider / neutrino factory, ablation of pellets in tokamaks, and processes in hybrid magnetoinertial fusion.

Keywords: Front tracking, multiphase MHD, liquid metal MHD

1. Introduction

MHD of liquid metals and conducting liquid salts attracts considerable attention from researchers because of their current and potential applications in fusion energy research, accelerator sciences, and industrial processes. Applications such as liquid wall plasma facing components (PFCs) in devices for magnetically confined fusion (tokamaks) [1] - [2], liquid metal targets for future particle accelerators [3], etc., motivate the study of free surface magnetohydrodynamic flows either in vacuum or non-conducting media.

Among other codes developed to study such physical problems, we would like to single out HIMAG and compressible FronTier-MHD. The HIMAG code [4] (HyPerComp Incompressible MHD solver for Arbitrary Geometries) is developed to model the flow of liquid metal with free surfaces in the presence of strong multi-component magnetic fields. It uses hybrid meshes comprising of hex, prism and tet elements, and the level set technique for the free surface support. But the diffusive nature of the level set method that replaces the density discontinuity across material interfaces by a continuous density function and smears the discontinuity across several mesh blocks limits the accuracy for problems involving large density discontinuities.

*Corresponding author. Tel.: +1-631-632-8353 ; fax: +1-631-632-8490 .
E-mail address: roman.samulyak@stonybrook.edu.

Selection and peer review under responsibility of the organizers of the 2013 International Conference on Computational Science
doi:10.1016/j.procs.2013.05.215

The compressible FronTier-MHD code [5], developed by one of the authors and collaborators as an extension of the hydrodynamic code FronTier [11], employs the method of front tracking [13] for material interfaces, second order hyperbolic solvers for equations of compressible fluids, and the embedded boundary method for the elliptic problem in complex domains. The FronTier code always keeps discontinuities sharp and eliminates or strongly restricts numerical diffusion across material interfaces. It supports large number of geometrically complex interfaces in two- and three-dimensional spaces and robustly resolves their topological changes. FronTier has been widely used for variety of fundamental science (turbulent fluid mixing [6]) and applied problems (liquid targets for particle accelerators [7], pellet ablation in tokamaks [8], and plasma jet liners for magneto-inertial fusion [9]). The code is well suited for free surface MHD phenomena driven by hydro waves, for instance in the case of matter interacting with strong energy sources. The obvious limitation of this code for the simulation of slow flows of liquid metals is the restriction of time steps by the CFL condition due to acoustic waves.

In order to overcome this limitation but keep all advantages of front tracking, we have developed a sharp interface MHD algorithm for incompressible multiphase MHD flows in the low magnetic Reynolds number approximation. As the method is dependent on the quality of the Navier-Stokes equation solver, we would like to comment first on the hydrodynamic component of the code. Front tracking has already been used for the simulation of incompressible Navier-Stokes equations [14, 15]. But unlike the front tracking method for compressible flows [11] which always keeps the density discontinuity sharp, previous implementations of the front tracking for incompressible flows employed the smoothing of density similar to the level set method. Other methods such as the ghost fluid method [16, 17] and the immersed interface method [18, 19] also have difficulties with large density ratios across the interface. A front tracking algorithm for incompressible Navier-Stokes approximations that successfully deals with the large density discontinuity problem has been recently proposed by authors and collaborators [20] by using the embedded boundary method [21] .

In this paper, we describe a front tracking MHD algorithm for free surface / multiphase flows in the low magnetic Reynolds number approximation, coupled with the incompressible hydrodynamic solver, as well as validation and verification tests. With the advantage of incompressible hydrodynamic solver, the code can deal with the simulation of large time scales, in particular, with flows of free surface liquid metals in magnetic fields.

The paper is organized as follows. The governing equations and approximations are discussed in Section 2. In Section 3, the numerical algorithm and implementation are described. The verification and validation test is presented in Section 4. We briefly describe applications of the code in the area of accelerator targets in Section 5. Finally, we conclude the paper withe the summary of our results and perspectives for the future work.

2. Governing Equations

We are interested in the description of multiphase or multi-material systems involving conducting fluids interacting with neutral fluids or gases in the presence of magnetic fields. Interfaces of the phase or material separation are assumed to be sharp (the thickness of the interface is negligible) and, in general, geometrically complex. The numerical simulation of liquid metals, liquid salts, and weakly ionized plasmas, which are relatively weak electrical conductors, is difficult using the standard full systems of MHD equations [12]. Fast diffusion of the magnetic field, caused by low value of electrical conductivity, introduces unwanted small time scales into the problem. If the time scale of the diffusion of the magnetic field is small compared to hydrodynamic time scale, the magnetic Reynolds number [24]

$$Re^M = \frac{4\pi u \sigma L}{c^2},$$

where L is the typical length scale, u is the fluid velocity, and σ is the electric conductivity, is small. If, in addition, the eddy-current-induced magnetic field δB is small compared to the external field B, the full system of MHD equations can be simplified by neglecting the time evolution of the magnetic field. In this case, the generalized Ohm's law is used for the evaluation of the current-density distribution instead of the Maxwell equation $\mathbf{J} = \frac{c}{4\pi}\nabla \times \mathbf{H}$, where the magnetic field $\mathbf{H}$ and the magnetic induction $\mathbf{B}$ are related by the magnetic permeability coefficient μ: $\mathbf{B} = \mu\mathbf{H}$. The governing equations of incompressible conductive fluids in the low magnetic Reynolds

number approximation are

$$\rho\left(\frac{\partial}{\partial t}+\mathbf{u}\cdot\nabla\right)\mathbf{u} = \mu\Delta\mathbf{u}-\nabla P+\rho g+\frac{1}{c}(\mathbf{J}\times\mathbf{B}) \quad (1)$$

$$\nabla\cdot\mathbf{u} = 0 \quad (2)$$

$$\mathbf{J} = \sigma\left(-\nabla\varphi+\frac{1}{c}\mathbf{u}\times\mathbf{B}\right) \quad (3)$$

$$\nabla\cdot\mathbf{J} = 0 \quad (4)$$

Taking the divergence of both sides of equation (3) together with equation (4), an elliptic equation for the electric potential is obtained:

$$\nabla\cdot(\sigma\nabla\varphi) = \nabla\cdot\frac{\sigma}{c}(\mathbf{u}\times\mathbf{B}) \quad (5)$$

If a conductive fluid interfaces a neutral fluid or gas, the current density vector is tangential to the material interface. This statement is expressed by the following Neumann boundary condition for the Poisson equation (5).

$$\left.\frac{\partial\varphi}{\partial\mathbf{n}}\right|_{\Gamma} = \left.\frac{1}{c}(\mathbf{u}\times\mathbf{B})\cdot\mathbf{n}\right|_{\Gamma} \quad (6)$$

where Γ is the boundary of conductive fluid.

3. Numerical Algorithm and Implementation

The proposed numerical algorithm uses the method of front tracking for the propagation of material interfaces and the embedded interface method for elliptic problems associated with an implicit discretization of the incompressible Navier-Stokes equations (1) - (2) and the Poisson problem for the electric potential (5) - (6). The task is complicated by the fact that these elliptic problems contain either geometrically complex outside boundary or an interior surface across which large discontinuities of material properties or solutions occur. Within the method of front tracking, the fluid interface is represented as an explicit co-dimension one Lagrangian mesh moving through a volume filling Eulerian mesh.

3.1. Elliptic Interface Problem

The embedded boundary method (EBM) for irregular domains [21, 22] was extended by the authors ([26]) to solve the elliptic and parabolic interface problem with interior boundaries. In general form, the elliptic partial differential equation is

$$\nabla\cdot\beta\nabla T = f \quad (7)$$

where the function β is continuous and smooth except at the interior boundary and f is a given function, continuous except perhaps at the interior boundary. Boundary conditions for both exterior and interior boundary are needed to close the problem. The boundary condition for the exterior boundary is either of Dirichlet or Neumann type. At the interior boundary, the following jump conditions are applied:

$$[T] = J_1 \quad (8)$$

$$\left[\beta\frac{\partial p}{\partial n}\right] = J_2 \quad (9)$$

The embedded boundary method is a finite volume method for an irregular domain embedded on a Cartesian grid. When embedded boundary method is used to solve the elliptic boundary value problem, unknowns are defined in the computational cell centers for both interior cells (full cells) as well as boundary cells (partial cells) which intersect with the interior boundary, instead of being defined in the geometrical center of a cell ([26, 21, 22, 25]). This main feature of EBM is retained in the algorithm for the elliptic interface problem. For a full cell, one unknown is set at the cell center and the standard finite volume method is used to obtain one linear algebraic

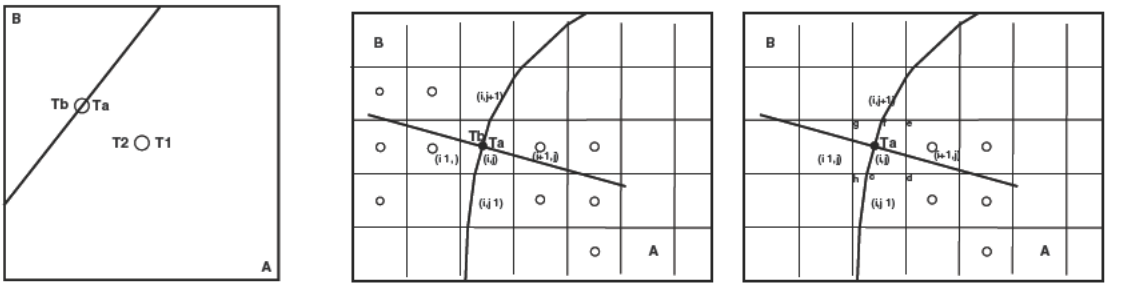

(a) (b) (c)

Fig. 1. (a) Placement of unknowns in a cell containing the interface, (b) stencil for the interface unknowns for the jump condition, and (c) stencil for the cell center unknowns.

equation. On the other hand, more unknowns are needed in order to discretize the elliptic equation consistent with two interface jump conditions for partial cells. Figure 1a shows the placement of unknowns in a cell with interior boundary. The whole cell contains two partial cells representing two material components (A and B) which are separated by the interior boundary. Two unknowns (T_1, T_2) are defined in the cell center for each part of the cell. In order to satisfy the jump conditions (8) and (9), two additional unknowns T_a and T_b are defined in the geometrical center of the segment of the interior boundary intersecting with the cell.

While the algorithm implemented in the code works in both two- and three-dimensional spaces, we focus here on a two-dimensional case for visual simplicity. A schematic of the corresponding stencil for the interpolation of boundary unknowns is shown in Figure 1b. The direction of the normal vector to the interior boundary is from A to B, assuming that A is the interior component. The discretization of the jump condition (8) is simply

$$T_A - T_B = J_1 \tag{10}$$

The discretization of the jump condition (9) is more complicated because the normal derivatives of unknowns in both sides of the interior boundary have to be calculated. This is processed by fitting a quadratic polynomial ([21, 22]). The main idea is to use one unknown in cell (i,j), two unknowns in the first layer of neighbors of cell (i,j), and three unknowns in the second layer of neighbors of cell (i,j), that six unknowns in total are given for six coefficients of the quadratic polynomial. For example, in order to construct the quadratic polynomial to evaluate the flux at the interior boundary segment center for component A, the six unknowns are T_a, $T_{i+1,j}$, $T_{i+1,j-1}$, $T_{i+2,j}$, $T_{i+2,j-1}$, and $T_{i+2,j-2}$. Similarly, we can construct the quadratic polynomial for component B. Taking the normal derivatives of the fitted polynomials for two components to obtain $\frac{\partial T}{\partial \mathbf{n}}\big|_A$, $\frac{\partial T}{\partial \mathbf{n}}\big|_B$, respectively, and using the jump condition (9), we obtain,

$$\beta|_B \left.\frac{\partial T}{\partial \mathbf{n}}\right|_B - \beta|_A \left.\frac{\partial T}{\partial \mathbf{n}}\right|_A = J_2 \tag{11}$$

The embedded boundary method is used to setup two equations for two unknowns in the cell center separately. For the partial cell $cdef$, a similar stencil is used to discretize the elliptic operator (see Figure 1c). Integrating equation (7) and using the divergence theorem, we obtain

$$\int_{cdef} \nabla \cdot (\beta \nabla T)\, ds = \oint_{\partial(cdef)} \beta \nabla T \cdot \mathbf{n}\, dl = \int_{cdef} f\, ds \tag{12}$$

which is

$$\int_{cd} \beta \nabla T \cdot \mathbf{n}\, dl + \int_{de} \beta \nabla T \cdot \mathbf{n}\, dl + \int_{ef} \beta \nabla T \cdot \mathbf{n}\, dl + \int_{fc} \beta \nabla T \cdot \mathbf{n}\, dl = \int_{cdef} f\, ds. \tag{13}$$

The discretized form is

$$l_{cd} \cdot Flux_{cd} + l_{de} \cdot Flux_{de} + l_{ef} \cdot Flux_{ef} + l_{fc} \cdot Flux_{fc} = f(i,j) \int_{cdef} ds \tag{14}$$

where l_{xy} is the length of the segment between x and y. For $Flux_{cd}$, a second order derivative is calculated by using the linear interpolation of $\frac{T_{i,j-1}-T_{i,j}}{\Delta x}$ and $\frac{T_{i+1,j-1}-T_{i+1,j}}{\Delta x}$ in the center of segment cd [21] and multiplying by β. For $Flux_{de}$, we simply use central difference $\frac{T_{i+1,j}-T_{i,j}}{\Delta y}$ to calculate the derivative and multiply β. $Flux_{ef}$ is obtained similarly to $Flux_{cd}$ by evaluating linear interpolation of $\frac{T_{i,j+1}-T_{i,j}}{\Delta x}$ and $\frac{T_{i+1,j+1}-T_{i+1,j}}{\Delta x}$ in the center of ef and multiplying by β. $Flux_{fc}$ is evaluated, as described in the previous paragraph, as $\beta|_A \left.\frac{\partial T}{\partial \mathbf{n}}\right|_A$. Similarly, fluxes of other partial cells are obtained. As the unknowns at the geometrical centers of interface segments can be expressed in terms of unknowns in cell centers, the resulting system of equations is written only for unknowns defined at cell centers.

The 3D algorithm is similar. A bi-linear interpolation is used for the interface fluxes and 10 unknowns are used to construct a quadratic polynomial in 3D containing 10 coefficients.

3.2. Hydro- and MHD Algorithms

The system of MHD equations (1)−(4), a coupled parabolicelliptic system in a geometrically complex domain, is solved using operator splitting and front tracking. The propagation and redistribution of the interface using the method of front tracking ([11],[13]) is performed at the beginning of each time step. Interfaces are represented by triangle meshes that are propagated in each time step. The topology issues of the interface are resolved by the FronTier library and the only information required by the FronTier library is the discretized velocity filed in the computational domain, which is stored in the center of each computation grid. Velocity of each vertex in the interface mesh is the result of interpolation of nearby cell center velocities. Then interior states are updated by the incompressible hydro solver.

The magnetic source term ($\frac{1}{c}(\mathbf{J}\times\mathbf{B})$) is evaluated first. The discretization of equation (5) is similar to that in section (3.1), while the boundary condition is much simpler. Similarly, integrating equation (5) together with divergence theorem, we obtain.

$$\int_v \nabla\cdot(\nabla\varphi)\,dv = \oint_{\partial v} \nabla\varphi\cdot\mathbf{n}\,ds = \oint_{\partial v} \frac{1}{c}(\mathbf{u}\times\mathbf{B})\cdot\mathbf{n}\,ds, \tag{15}$$

which is

$$\oint_{\partial v} \frac{\partial\varphi}{\partial\mathbf{n}}\,ds \quad = \quad \oint_{\partial v} \frac{1}{c}(\mathbf{u}\times\mathbf{B})\cdot\mathbf{n}\,ds. \tag{16}$$

With the boundary condition (6), we can see that the integral along the boundary of conductive fluid in each partial cell is canceled in both sides of (16), and the discretization equation is greatly simplified.

After solving equation (5), the gradient of the electric potential φ is substituted into equation (3) and the current density $\mathbf{J}$ is obtained. Secondly, we deal with the equation (1), without regarding the divergence constraint, for an intermediate velocity $\mathbf{u}^*$. Employing an operator splitting technique, we resolve the advection step

$$\frac{\mathbf{u}^{'}-\mathbf{u}^n}{\Delta t} \quad = \quad -(\mathbf{u}^n\cdot\nabla)\mathbf{u}^n. \tag{17}$$

Only for the advection step, the density jump across the interface of two fluid components is smoothed with a certain smoothing radius of computation cells [14]. The advection part, equation (17), is evaluated explicitly, with a second order Godunov type scheme ([10]). For the diffusion part, we employ the implicit Crank-Nicolson method. Two fluid components are solved together, disregarding the interface.

Thirdly, the diffusion step and the source term are resolved

$$\frac{\mathbf{u}^*-\mathbf{u}^{'}}{\Delta t}+\nabla q \quad = \quad \rho g+\frac{1}{c}(\mathbf{J}\times\mathbf{B})+\frac{\mu}{2}\nabla^2(\mathbf{u}^*+\mathbf{u}^{'}), \tag{18}$$

where q is the pressure of the previous time step. Finally, we perform the projection step. Applying the divergence operator in both sides of equation

$$\mathbf{u}^* \quad = \quad \mathbf{u}^{n+1}+\frac{\Delta t}{\rho}\nabla\phi^{n+1} \tag{19}$$

and using the divergence constraint $\nabla \cdot \mathbf{u}^{n+1} = 0$, we obtain the following elliptic equation for pressure

$$\nabla^2 \phi^{n+1} = \frac{\rho}{\Delta t} \nabla \cdot \mathbf{u}^*. \tag{20}$$

The projection step is an elliptic interface problem discussed in section (3.1). Two jump conditions for pressure are

$$[p] = \sigma\kappa \tag{21}$$

$$\left[\frac{1}{\rho}\frac{\partial p}{\partial \mathbf{n}}\right] = 0 \tag{22}$$

where κ is the curvature and σ is the surface tension coefficient. A matrix to solve such elliptic interface problem is set according to the algorithm described in section (3.1).

The pressure is updated using the solution of the projection step:

$$p = q + \phi^{n+1} \tag{23}$$

The described algorithm achieves the second order convergence.

The implementation is carried out with C++ and MPI for the communication between processors. FronTier's hyperbolic solvers demonstrate good scalability on large machines of the IBM BlueGene series. The scalability of elliptic solvers is determined by the scalability of commonly used parallel libraries for sparse linear system of equations (preconditioned Krylov subspace iterative solvers of the PETSc library have been used in our MHD code).

4. Verification and Validation

Verification and validation tests for the three-dimensional FronTier-MHD code have been performed using experimental and theoretical studies of liquid mercury jets in magnetic fields. Experimental studies of a mercury jet entering a magnetic field with the magnitude satisfying the hyperbolic tangent profile have been performed in [23]. An asymptotic theoretical analysis has also been done by the same group. The experiment setup is as follows. A mercury jet with the initial diameter of 8 mm is shot horizontally into a transverse magnetic field with the initial velocity of 2.1 m/s. The amplitude of the transverse magnetic field satisfies the following equation

$$(\frac{B_y}{B_{max}})^2 = \frac{1}{2}[1 - \tanh(\frac{z - z_0}{L_m})], \tag{24}$$

where z_0 is the center and L_m is the characteristic length of the magnetic field. In our simulations, $z_0 = 1.5$ cm and $L_m = 0.62$ cm.

As predicted in [23], the magnitude of expansion of the jet depends on the z value:

$$\begin{aligned} g^*_{s2}(z'^*) &= \beta sin(\alpha z'^*) \int_{-\infty}^{z'^*} \frac{cos(\alpha t)}{cosh^2(\varepsilon_m t)}\, dt \\ &\quad -\beta cos(\alpha z'^*) \int_{-\infty}^{z'^*} \frac{cos(\alpha t)}{cosh^2(\varepsilon_m t)}\, dt \end{aligned} \tag{25}$$

where $\alpha = \sqrt{6/W_a}$ and $\beta = \varepsilon_m N_a / 8\alpha$. And

- $N_a = \sigma_e B^2_{max} a/\rho_f \omega_0$ is the Stuart number of the jet, σ_e is the electric conductivity of mercury, a is the radius of the cross-section of the jet, ρ_f is the density of mercury and ω_0 is the main flow velocity which is 2.1m/s.
- $W_a = \rho_f a \omega_0^2/\sigma$ is the Weber number of the jet, σ is the surface tension of mercury.
- $\varepsilon_m = a/L_m$ and $z'^* = z/a$.

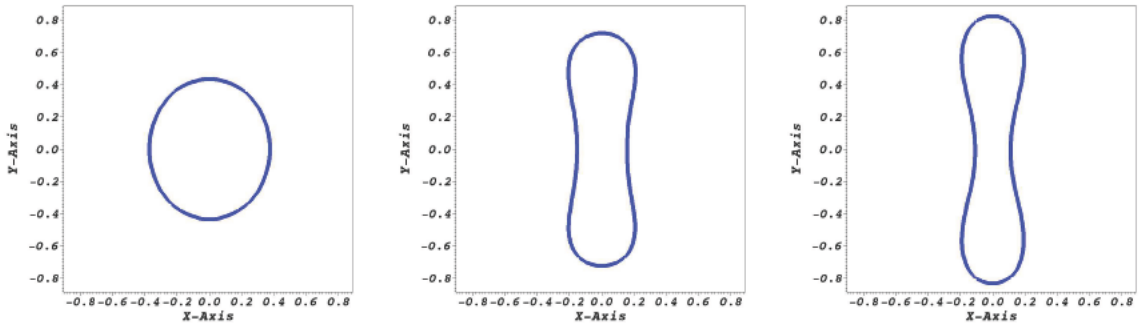

Fig. 2. FronTier-MHD simulation of jet deformation in magnetic field. Cross sections of the jet are shown at observation points located at 0, 3.5, and 5.5 cm.

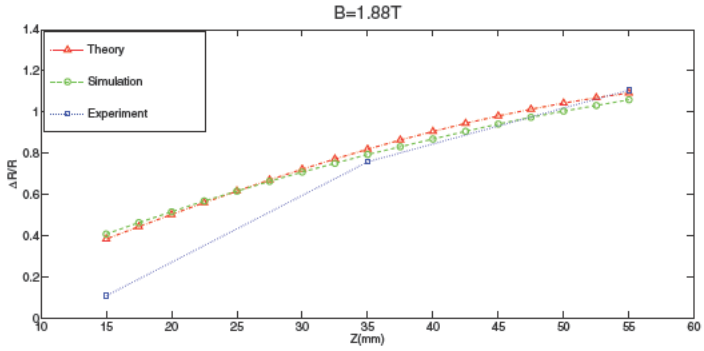

Fig. 3. Mercury jet deformation as function of the distance from the magnetic field center for 1.88 T magnetic field. Results of simulations (green dashed line), asymptotic calculations (red dash-dotted line), and experiments (blue dotted line) are shown.

Numerical simulation was performed using the magnetic filed strength B_{max} of 1.41 T and 1.88 T. In order to save computation time, simulations were performed in a frame moving with the initial jet velocity. In the asymptotic analysis of [23], the jet was assumed to extend infinitely and reach the steady state. To simulate similar conditions, initially long cylindrical jet was moving through the magnetic field rather then being ejected from the nozzle. Also, the jet is assumed to be in the vacuum while in the simulation, the vacuum was substituted with light gas, with the density 10^4 times smaller than the density of mercury. With such a large density ratio, the influence of gas on the momentum of the mercury jet can be ignored. In order to obtain accurate profile of the electric current density, the computational mesh contained approximately 20 cells across the cross-section of the mercury jet.

Experimental results of the jet deformation from [23], results of asymptotic analysis, and numerical simulations are plotted in Figure 3 for 1.88 T magnetic field and in Figure 4 for 1.41 T field. We observe a very good agreement of simulations with asymptotic calculations at small distances from the magnetic field center corresponding to smaller jet deformations. The expected disagreement with experimental results at small distances can be explained by the fact that experiments were carried out using a cylindrical nozzle located at $z = 0$ that reduced jet deformations compared to long free jets. But at larger distances from the nozzle corresponding to larger jet deformations, numerical simulations, theoretical calculations, and experiments are all in agreement.

We would like to comment on the importance of maintaining a sharp density discontinuity via the front tracking and embedded boundary methods. Without the embedded boundary method, the density ratio that interior solving can handle is limited by high condition number of the corresponding matrix of projection step. In order to perform the simulation without the embedded boundary method, we artificially increased the density of ambient gas so

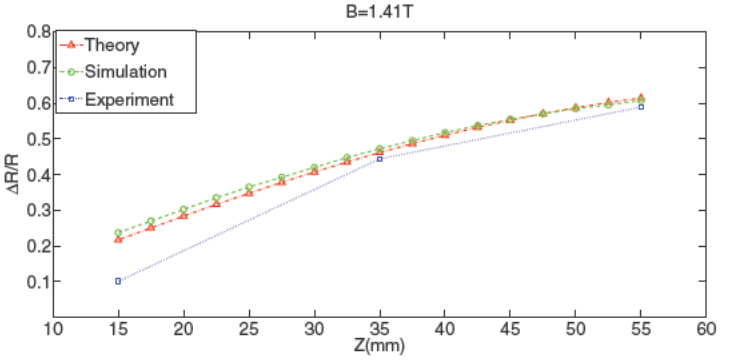

Fig. 4. Mercury jet deformation as function of the distance from the magnetic field center for 1.41 T magnetic field. Results of simulations (green dashed line), asymptotic calculations (red dash-dotted line), and experiments (blue dotted line) are shown.

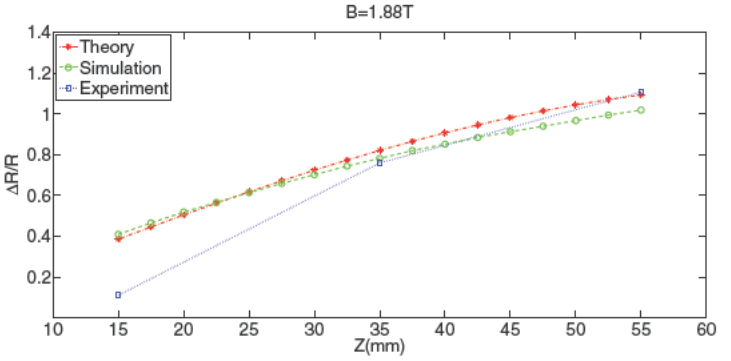

Fig. 5. Degradation of accuracy without sharp density discontinuity. Mercury jet deformation as function of the distance from the magnetic field center for 1.88 T magnetic field. Results of untracked simulations (green dashed line), asymptotic calculations (red dash-dotted line), and experiments (blue dotted line) are shown.

that the density ratio dropped to 10. Figures 5 and 6 demonstrate the degradation of accuracy of simulations if the correct density ratio and sharp density discontinuity are not resolved. Keeping the discontinuity sharp is even more important for applications involving more extreme flow regimes.

5. Applications

Both compressible and incompressible fluid FronTier-MHD code are used for the simulation of processed relevant to energy research and accelerator applications. Simulations of the mercury target for the Muon Accelerator Project (http://map.fnal.gov) is among the most important applications of the code. The target will contain a series of 30-cm-long and 1-cm-diameter mercury jets entering a strong ($\sim$ 15 Tesla) magnetic field at a small angle to the solenoid axis. When each jet reaches the center of the solenoid, it interacts with a powerful proton pulse penetrating the jet and depositing energy of the order of 100 J/g into mercury. The purpose of our numerical simulations is to evaluate states of the target before and after the interaction with protons to optimize the target design. The compressible code deals with the jet instabilities due to external energy deposition and their partial stabilization by the magnetic field [7]. The incompressible FronTier MHD code is used for the simulation of liquid metal jets in magnetic fields of different configurations prior to the interaction with proton pulses. Other applications involve pellet ablation in tokamaks [8], and plasma jet liners for magneto-inertial fusion [9].

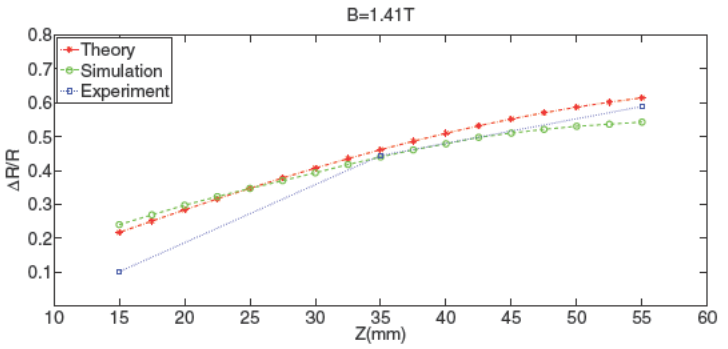

Fig. 6. Degradation of accuracy without sharp density discontinuity. Mercury jet deformation as function of the distance from the magnetic field center for 1.41 T magnetic field. Results of untracked simulations (green dashed line), asymptotic calculations (red dash-dotted line), and experiments (blue dotted line) are shown.

6. Conclusions

A numerical algorithm and the parallel FronTier-MHD code for the study of three-dimensional, incompressible, multiphase or free surface MHD flows at low magnetic Reynolds numbers, capable of handling large density ratios across material interfaces, have been developed. The algorithm is based on the front tracking method for material interfaces and the embedded boundary methods for elliptic problems. The code has achieved a good accuracy in verification and validation tests involving three-dimensional mercury jets in nonuniform magnetic fields. The FronTier-MHD code has been used for simulations of liquid mercury targets for the proposed muon collider / neutrino factory, ablation of pellets in tokamaks, and processes in hybrid magnetoinertial fusion.

Acknowledgments:
This work was supported in part by the Muon Accelerator Program of the US Department of Energy.

References

[1] A. Y. Ying, N. B. Morley, S. Smolentsev, K. Gulec, P. Fogarty, Free surface heat transfer and innovative designs for thin and thick liquid walls, Fusion Engineering and Design, Vol. 49-50, pp. 397- 406, 2000
[2] M. Abdou, N. Morley, M. Sawan, Editors, Special Issue on Innovative High-Power Density Concepts for Fusion Plasma Chambers, Fusion Engineering and Design, Vol. 72, Issues 1-3, pp. 1-326, November, 2004
[3] K. McDonald *et al.*, The MERIT high-power target experiment at the CERN PS, Proc. PAC09 (Vancouver, Canada), TU4GRI03, 2009.
[4] M.-Jiu Ni, R. Munipalli, N. B. Morley, M. A. Abdou, Validation strategies of HIMAG in interfacial flow computation for fusion applications, Fusion Engineering and Design, Vol. 81, 2006, 1535 - 1541.
[5] R. Samulyak, J. Du, J. Glimm, and Z. Xu. A numerical algorithm for MHD of free surface flows at low magnetic reynolds numbers. *J. Comput. Phys.*, 226:1532–1546, 2007.
[6] H. Lim, J. Iwerks, Y. Yu, J. Glimm, and D. H. Sharp. Verification and validation of a method for the simulation of turbulent mixing. *Physica Scripta*, T142:014014, 2010.
[7] R. Samulyak, W. Bo, X. Li, H. Kirk, and K. McDonald. Computational algorithms for multiphase magnetohydrodynamics and applications. *Condensed Matter Physics*, 13:43402, 2010.
[8] R. Samulyak, T. Lu, and P. Parks. A hydromagnetic simulation of pellet ablation in electrostatic approximation. *Nuclear Fusion*, 47:103–118, 2007.
[9] H. Kim, L. Zhang, R. Samulyak, P. Parks, On the structure of plasma liners for plasma jet induced magnetoinertial fusion. *Phys. Plasmas*, 2013. In press.
[10] J. B. Bell, P. Colella, and H. M. Glaz. A second order projection method for the incompressible navier-stokes equations. *J. Comput. Phys.*, 85:257, 1989.
[11] J. Du, B. Fix, J. Glimm, X. Jia, X. Li, Y. Li, and L. Wu. A simple package for front tracking. *J. Comput. Phys.*, 213:613 – 628, 2006.
[12] J. P. FREIDBERG. *Rev. Mod. PHys.*, 54:801, 1982.
[13] J. Glimm, J. Grove, X. Li, K. L. Shyue, Q. Zhang., and Y. Zeng. Three dimensional front tracking. *SIAM J. Sci. Comput.*, 19:703–727, 1998.
[14] S. O. Unverdi and G. Tryggvason. A front-tracking method for viscous, imcompressible, multi-fluid flows. *J. Comput. Phys.*, 100(1):25–37, 1992.
[15] G. Tryggvason, B. Bunner, and et. al. A front-tracking method for the computations of multiphase flow. *J. Comput. Phys.*, 169:708–759, 2001.

[16] X.-D. Liu, R. Fedkiw, and M. Kang. A boundary condition capturing method for poisson's equation on irregular domains. *J. Comput. Phys.*, 160:151–178, 2000.
[17] M. Kang, R. Fedkiw, and X.-D. Liu. A boundary condition capturing method for multiphase incompressible flow. *J. Sci. Comput.*, 15(3):323–360, 2000.
[18] Z. Li and K. Ito. *The Immersed Interface Method: Numerical Solutions of PDEs Involving Interfaces and Irregular Domains*. Frontiers Appl. Math. 33, SIAM, Piladelphia, 2006.
[19] L. Lee and R. LeVeque. An immersed interface method for incompressible navier-stokes equations. *SIAM J. Sci. Comput.*, 25(3):832–856, 2003.
[20] S. Wang, J. Glimm, R. Samulyak, X. Jiao, Embedded boundary method for two phase incompressible flow, 2012. Submitted, available at arxiv.ogr
[21] H. Johansen and P. Colella. A cartesian grid embedding boundary method for Poisson's equation on irregular domains. *J. Comput. Phys.*, 147:60–85, 1998.
[22] P. McCorquodale, P. Colella, and H. Johansen. A cartesian grid embedded boundary method for the heat equation on irregular domains. *J. Comput. Phys.*, 173:620–635, 2001.
[23] S. Oshima, R. Yamane, Y. Moshimaru, and T. Matsuoka. The shape of a liquid metal jet under a non-uniform magnetic field. *JCME Int. J.*, 30:437C448, 1987.
[24] C. B. Reed S. Molokov. Review of free-surface mhd experiments and modeling. Technical Report ANL/TD/TM99-08, Argonne National Laboratory, 1999.
[25] P. Schwartz, M. Barad, P. Colella, T. Ligocki. A cartesian grid embedded boundary method for the heat equation and Poisson's equation in three dimensions. *J. Comput. Phys.*, 211:531–550, 2006.
[26] S. Wang, R. Samulyak, T. Guo. An embedded boundary method for elliptic and parabolic problems with interfaces and application to multi-material systems with phase transitions. *Acta Mathematica Scientia*, 30(2):499–521, 2010.